Original Article | Neuroimaging and Head & Neck

eISSN 2005-8330
https://doi.org/10.3348/kjr.2022.0732
Korean J Radiol 2023;24(2):133-144

Korean Journal of Radiology
KJR

Qualitative and Quantitative Magnetic Resonance Imaging Phenotypes May Predict CDKN2A/B Homozygous Deletion Status in Isocitrate Dehydrogenase-Mutant Astrocytomas: A Multicenter Study

Yae Won Park[1], Ki Sung Park[2], Ji Eun Park[3], Sung Soo Ahn[1], Inho Park[4, 5], Ho Sung Kim[3], Jong Hee Chang[6], Seung-Koo Lee[1], Se Hoon Kim[7]

[1]Department of Radiology and Research Institute of Radiological Science and Center for Clinical Imaging Data Science, Yonsei University College of Medicine, Seoul, Korea; [2]Department of Mechanical Engineering, Pohang University of Science and Technology, Pohang, Korea; [3]Department of Radiology, Ulsan University College of Medicine, Seoul, Korea; [4]Center for Precision Medicine, Gangnam Severance Hospital, Yonsei University College of Medicine, Seoul, Korea; [5]Department of Pathology, Gangnam Severance Hospital, Yonsei University College of Medicine, Seoul, Korea; Departments of [6]Neurosurgery and [7]Pathology, Yonsei University College of Medicine, Seoul, Korea

Objective: Cyclin-dependent kinase inhibitor (CDKN)2A/B homozygous deletion is a key molecular marker of isocitrate dehydrogenase (IDH)-mutant astrocytomas in the 2021 World Health Organization. We aimed to investigate whether qualitative and quantitative MRI parameters can predict CDKN2A/B homozygous deletion status in IDH-mutant astrocytomas.
Materials and Methods: Preoperative MRI data of 88 patients (mean age ± standard deviation, 42.0 ± 11.9 years; 40 females and 48 males) with IDH-mutant astrocytomas (76 without and 12 with CDKN2A/B homozygous deletion) from two institutions were included. A qualitative imaging assessment was performed. Mean apparent diffusion coefficient (ADC), 5th percentile of ADC, mean normalized cerebral blood volume (nCBV), and 95th percentile of nCBV were assessed via automatic tumor segmentation. Logistic regression was performed to determine the factors associated with CDKN2A/B homozygous deletion in all 88 patients and a subgroup of 47 patients with histological grades 3 and 4. The discrimination performance of the logistic regression models was evaluated using the area under the receiver operating characteristic curve (AUC).
Results: In multivariable analysis of all patients, infiltrative pattern (odds ratio [OR] = 4.25, p = 0.034), maximal diameter (OR = 1.07, p = 0.013), and 95th percentile of nCBV (OR = 1.34, p = 0.049) were independent predictors of CDKN2A/B homozygous deletion. The AUC, accuracy, sensitivity, and specificity of the corresponding model were 0.83 (95% confidence interval [CI], 0.72–0.91), 90.4%, 83.3%, and 75.0%, respectively. On multivariable analysis of the subgroup with histological grades 3 and 4, infiltrative pattern (OR = 10.39, p = 0.012) and 95th percentile of nCBV (OR = 1.24, p = 0.047) were independent predictors of CDKN2A/B homozygous deletion, with an AUC accuracy, sensitivity, and specificity of the corresponding model of 0.76 (95% CI, 0.60–0.88), 87.8%, 80.0%, and 58.1%, respectively.
Conclusion: The presence of an infiltrative pattern, larger maximal diameter, and higher 95th percentile of the nCBV may be useful MRI biomarkers for CDKN2A/B homozygous deletion in IDH-mutant astrocytomas.
Keywords: *Cyclin-dependent kinase inhibitor; Glioma; Magnetic resonance imaging; Radiogenomics*

INTRODUCTION

One of the major changes in the 2021 World Health Organization (WHO) classification of gliomas is the advanced role of molecular diagnostics in diagnosing isocitrate dehydrogenase (IDH)-mutant astrocytomas [1]. In

Received: September 29, 2022 **Revised:** November 22, 2022 **Accepted:** December 10, 2022
Corresponding author: Se Hoon Kim, MD, PhD, Department of Pathology, Yonsei University College of Medicine, 50-1 Yonsei-ro, Seodaemun-gu, Seoul 03722, Korea.
• E-mail: paxco@yuhs.ac

the presence of cyclin-dependent kinase inhibitor (CDKN)2A/B homozygous deletion, IDH-mutant histological grade 2 or 3 astrocytomas are designated grade 4, even in the absence of microvascular proliferation or necrosis [1,2]. This is based on the fact that histologic grading criteria alone may not stratify prognosis in IDH-mutant astrocytomas [3-6], and CDKN2A/B homozygous deletion has been proven to be an independent prognostic marker in all grades of IDH-mutant astrocytomas, including IDH-mutant grade 4 astrocytomas [3,7,8].

CDKN2A is a tumor suppressor gene located on chromosome 9p, band p21.3, which encodes the cell cycle inhibitors p14 and p16 [9]. The p14 protein activates the "guardian of the genome" p53, which plays an important role in apoptosis and DNA repair [10]. The p16 protein controls cell division by binding to cyclin-dependent kinases, thus blocking cell cycle progression from the G1 phase to the S phase [7]. The inactivation of tumor suppressor genes by deletion promotes the cell cycle and induces oncogenesis and tumor progression [11]. Currently, young patients with histological lower-grade IDH-mutant astrocytomas are often initially observed after gross total resection because earlier reports have indicated an absence of survival benefit with early radiation-based intervention [12]. However, the aggressive phenotype associated with CDKN2A/B homozygous deletion warrants a different approach. Thus, non-invasive imaging predictors of CDKN2A/B homozygous deletion status in IDH-mutant astrocytomas may further improve clinical decision-making by planning an aggressive surgical approach and predicting prognosis.

MRI is the most reliable imaging modality for brain tumor diagnosis and provides not only geographic spatial characteristics but also information on tumor phenotypes with qualitative and quantitative imaging features. Qualitative imaging features can be obtained using simple methods and have been proven to be biologically relevant in gliomas [13]. Quantitative features include the apparent diffusion coefficient (ADC) of diffusion-weighted imaging (DWI), which is an index of tumor cell density and reflects the tumor burden, whereas dynamic susceptibility contrast (DSC) imaging allows for the measurement of cerebral blood volume (CBV), which is a noninvasive marker for vasculature and tumor angiogenesis [14-16]. We hypothesized that a comprehensive evaluation of qualitative and quantitative markers may help predict CDKN2A/B homozygous deletion status in IDH-mutant astrocytomas.

Therefore, this study aimed to evaluate whether qualitative and quantitative MRI parameters can predict CDKN2A/B homozygous deletion status in IDH-mutant astrocytomas.

MATERIALS AND METHODS

Patient Population

This retrospective study was approved by the Institutional Review Board (IRB No. 4-2021-1381), and the requirement for informed consent was waived. The inclusion criteria for our study were as follows: 1) IDH-mutant astrocytomas confirmed by histopathology, 2) patients with known CDKN2A/B homozygous deletion status, and 3) age > 18 years. Patients with missing MRI sequences (n = 2) were excluded from this study. Between March 2020 and May 2022, 88 patients with pathologically diagnosed IDH-mutant astrocytomas were included in this study: 54 from the first institution (Severance Hospital) and 34 from the second institution (Asan Medical Center). A patient flowchart is shown in Figure 1.

Molecular Classification

All tissues were diagnosed according to the 2021 WHO classification [1]. Both immunohistochemical and peptide nucleic acid-mediated clamping polymerase chain reaction analyses were performed to detect the IDH1 R132H mutation [17]. In IDH1-negative cases, the IDH1/2 status was confirmed by a peptide nucleic acid-mediated clamping polymerized chain reaction. Fluorescent in situ hybridization analysis was used to investigate 1p/19q codeletion [18].

In the first institution, CDKN2A/2B homozygous deletions were inferred using a targeted Next-Generation Sequencing (NGS) gene panel assay (Illumina TruSight Oncology 500). From the TruSight Oncology 500 local-app pipeline (version 2), the CNV Robust Analysis For Tumors (CRAFT) copy number variant caller calculates fold-change values for each target region against the baseline coverages offered with the software. Cases having less than 0.5 of fold-change values of either CDKN2A or CDKN2B were selected for visual assessment to ensure that the low fold-change values of CDKN2A/2B are distinguishable from fold-change values of adjacent target regions. Visual assessment was performed on plots of the genome-wide copy number profile created from fold-change values of every target region of a sample using an in-house developed R script (Supplementary Fig. 1).

At the second institution, targeted NGS was performed

https://doi.org/10.3348/kjr.2022.0732

Korean Journal of Radiology
KJR

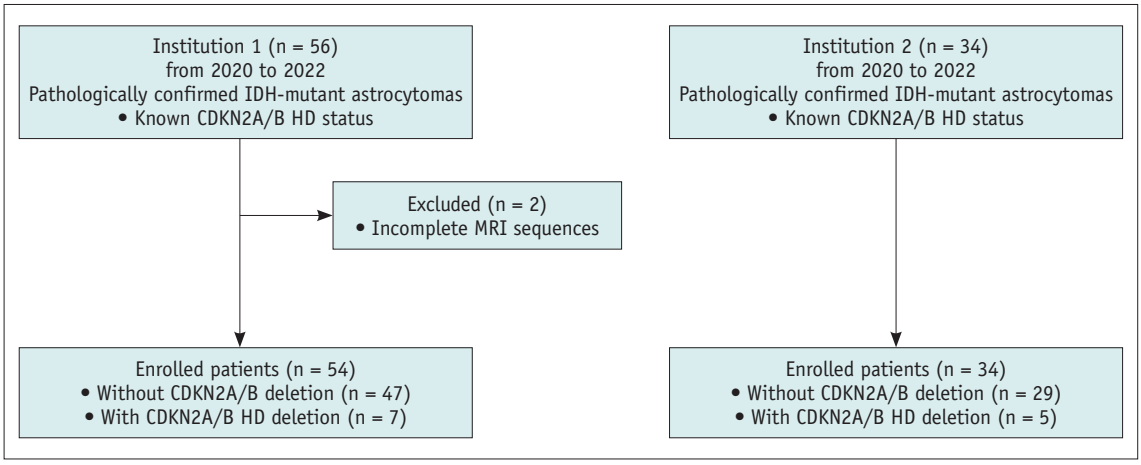

Fig. 1. Patient flowchart. CDKN = cyclin-dependent kinase inhibitor, HD = homozygous deletion, IDH = isocitrate dehydrogenase

using an Illumina NextSeq 500Dx panel. CDKN2A/2B homozygous deletions were inferred from copy number variations in high-throughput sequencing data from formalin-fixed cells using CNVkit12.

MRI Protocol

The preoperative MRI sequences included T1-weighted, T2-weighted, fluid-attenuated inversion recovery (FLAIR), and three-dimensional post-contrast T1-weighted images, as well as DWI and DSC images. Imaging was performed using 3T MRI scanners (Achieva or Ingenia, Philips Medical Systems). Details of the MRI protocols from the two institutions are provided in the Supplementary Material.

Preprocessing of DSC

A dedicated software (NordicICE; NordicNeuroLab) was used to process DSC images. According to the leakage correction method, leakage was estimated from the deviation of each voxel from a non-leakage reference tissue response curve [19]. Whole-brain relative CBV was also calculated. Normalization of the relative CBV (nCBV) was automatically performed using the mean value of the blood volume values outside the tumor without any intervention by the observers. Co-registration between the postcontrast T1-weighted (T1C) images and parametric maps from the DSC was performed automatically [20,21].

Conventional Imaging Analyses

For each patient, conventional imaging parameters, including the tumor location (frontal, temporal, insular, parietal, occipital, brainstem, and corpus callosum), cortical and corpus callosum involvement, ependymal extension, pial invasion, T2-FLAIR mismatch, the proportion of enhancing tumor > 33%, marked/avid enhancement, presence of a cyst, the proportion of necrosis > 5%, and infiltrative tumor, were assessed (Supplementary Table 1) [22,23]. Visual assessment was performed separately by two neuroradiologists (with 17 and 10 years of experience). In a rare case of ambiguity, a senior neuroradiologist (with 29 years of experience) was consulted.

Automatic Segmentation Process and Quantitative Analyses

Automatic segmentation was performed by applying the HD-GLIO brain tumor segmentation tool, which is an autosegmentation tool developed from a multi-institutional dataset [24,25], with a reported Dice coefficient of 0.95 in our previous dataset [26]. T1, T2, and FLAIR images were co-registered with T1C images. The total tumor (enhancing + non-enhancing hyperintense tumor) masks on the FLAIR images were used for further analysis. Enhancing or non-enhancing tumor masks were not separately analyzed because of the lack of a contrast-enhancing area in a portion of the patients.

The regions of interest (ROIs) were then transferred to the co-registered DWI and perfusion maps. The maximum diameter and volume were calculated from the ROIs. The mean value and 5th percentile values of ADC and the mean and 95th percentile values of nCBV were also calculated for the ROIs according to previous reports [27,28].

Statistical Analysis

The clinical and imaging characteristics were compared according to CDKN2A/B homozygous deletion status using

 https://doi.org/10.3348/kjr.2022.0732

the Chi-square test or Fisher's test for categorical variables and the independent samples *t* test or Mann-Whitney U test for continuous variables, according to normality. Interobserver agreement in the qualitative and quantitative imaging evaluations was calculated using Cohen's kappa index.

Among the clinical, conventional, and quantitative imaging parameters, significant variables were selected using univariable logistic regression. Variables of interest in the univariable analysis ($p < 0.05$) were included in the multivariable models using backward elimination according to the likelihood ratio with a variable selection criterion of $p < 0.05$. Variance inflation factor (VIF) was used to detect multicollinearity between variables, and all variables showed a VIF of less than 10. Receiver operating characteristic (ROC) curve analysis was performed to evaluate the discrimination performance of the corresponding logistic regression model, including the area under the curve (AUC). Youden's index was used to determine the cutoff for calculating accuracy, sensitivity, and specificity. Subgroup analysis was performed for histological grades 3 and 4 IDH-mutant astrocytomas due to the lack of patients with CDKN2A/B homozygous deletion in histological grade 2 IDH-mutant astrocytomas.

Statistical analyses were performed using the R software (version 3.3.1). Statistical significance was set at $p < 0.05$. Since our study was exploratory, no adjustment for multiple tests was performed.

RESULTS

Patient Characteristics

This study included a total of 88 patients (mean age ± standard deviation, 42.0 ± 11.9 years; 40 females and 48 males); 76 (86.4%) without CDKN2A/B homozygous deletion, and 12 (13.6%) with CDKN2A/B homozygous deletion. Forty-one (46.6%) patients had histological grade 2, 23 (26.1%) patients were histological grade 3, and 24 (27.3%) patients were histological grade 4. Fifty-eight (65.9%) patients underwent gross total resection, 27 (30.7%) patients underwent subtotal or partial resection, and three (3.4%) patients underwent biopsy.

Interobserver Agreement for Qualitative Imaging Analyses

The interobserver agreement between the two neuroradiologists for qualitative imaging parameters was excellent (κ range, 0.820–0.948) (Supplementary Table 2).

Clinical and Imaging Parameters for Predicting CDKN2A/B Homozygous Deletion Status in All IDH-Mutant Astrocytomas

IDH-mutant astrocytomas with CDKN2A/B homozygous deletion showed significantly different proportions of histological grade compared to those without CDKN2A/B homozygous deletion (proportions of grade 2, 3, and 4; 0%, 25.0%, and 75.0% in patients with CDKN2A/B homozygous deletion; 54.0%, 26.3%, and 19.7% in patients without CDKN2A/B homozygous deletion, $p < 0.001$). IDH-mutant astrocytomas with CDKN2A/B homozygous deletion showed larger proportions of corpus callosum involvement (50.0% vs. 9.2%, $p < 0.001$), ependymal extension (66.7% vs. 17.1%, $p < 0.001$), enhancing tumor > 33% (83.3% vs. 22.4%, $p < 0.001$), marked/avid enhancement (75.0% vs. 26.3%, $p = 0.001$), necrosis > 5% (50.0% vs. 13.2%, $p = 0.002$), infiltrative pattern (41.7% vs. 6.6%, $p = 0.002$), maximal diameter (8.12 cm vs. 5.70 cm, $p = 0.005$), volume (115.87 cm^3 vs. 56.58 cm^3, $p = 0.001$), and 95th percentile of nCBV (7.71 vs. 5.51, $p = 0.007$) than those of IDH-mutant astrocytomas without CDKN2A/B homozygous deletion. There were no significant differences in other clinical and imaging parameters (Table 1).

Table 2 shows results from the univariable and multivariable analyses. On univariable analysis, corpus callosum involvement (odds ratio [OR] = 9.86, $p = 0.001$), ependymal extension (OR = 9.69, $p = 0.001$), the proportion of enhancing tumor > 33% (OR = 17.35, $p = 0.001$), marked/avid enhancement (OR = 17.35 $p = 0.001$), the proportion of necrosis > 5% (OR = 6.60, $p = 0.005$), infiltrative pattern (OR = 10.14, $p = 0.002$), maximal diameter (OR = 1.06, $p = 0.004$), volume (OR = 1.02, $p = 0.003$), and 95th percentile of nCBV (OR = 1.27, $p = 0.012$) were predictors of CDKN2A/B homozygous deletion. On multivariable analysis, infiltrative pattern (OR = 4.25, $p = 0.034$), maximal diameter (OR = 1.07, $p = 0.013$), and 95th percentile of nCBV (OR = 1.34, $p = 0.049$) were independent predictors of CDKN2A/B homozygous deletion. The AUC, accuracy, sensitivity, and specificity of the multivariable model were 0.83 (95% [CI] 0.72–0.91), 90.4%, 83.3%, and 75.0%, respectively. Representative cases of IDH-mutant astrocytomas without and with CDKN2A/B homozygous deletion status are presented in Figures 2 and 3. ROC curves of the multivariable model are shown in Figure 4A.

https://doi.org/10.3348/kjr.2022.0732

Korean Journal of Radiology
KJR

Clinical and Imaging Parameters for Predicting CDKN2A/B Homozygous Deletion Status in the Subgroup with Histological Grades 3 and 4 IDH-Mutant Astrocytoma

In subgroup analysis, IDH-mutant astrocytomas with CDKN2A/B homozygous deletion showed larger proportions of corpus callosum involvement (50.0% vs. 14.3%, p = 0.012), ependymal extension (66.7% vs. 3.14%, p = 0.032), enhancing tumor > 33% (83.3% vs. 48.6%, p = 0.036), infiltrative pattern (41.7% vs. 11.4%, p = 0.022), maximal

Table 1. Comparison of Clinical, Pathological, and Imaging Parameters according to the CDKN2A/B Homozygous Deletion Status in IDH-Mutant Astrocytomas

	Without CDKN2A/B Homozygous Deletion (n = 76)	With CDKN2A/B Homozygous Deletion (n = 12)	*P**
Institution			0.817
Institution 1	47 (61.8)	7 (58.3)	
Institution 2	29 (38.2)	5 (41.7)	
Age, years	41.9 ± 11.9	42.3 ± 12.6	0.931
Sex, female	35 (46.1)	5 (41.7)	0.777
Histological grade			< 0.001
Grade 2	41 (54.0)	0 (0)	
Grade 3	20 (26.3)	3 (25.0)	
Grade 4	15 (19.7)	9 (75.0)	
Extent of resection			0.565
Gross total resection	51 (67.1)	7 (58.3)	
Subtotal or partial resection	22 (28.9)	5 (41.7)	
Biopsy	3 (3.9)	0 (0)	
MRI features			
Location			0.434
Frontal	42 (55.3)	9 (75.0)	
Temporal	11 (14.5)	2 (16.7)	
Insular	15 (19.7)	1 (8.3)	
Parietal	8 (10.5)	0 (0)	
Occipital	0 (0)	0 (0)	
Brainstem	0 (0)	0 (0)	
Corpus callosum	0 (0)	0 (0)	
Cortical involvement	72 (94.7)	11 (91.7)	0.669
Corpus callosum involvement	7 (9.2)	6 (50.0)	< 0.001
Ependymal extension	13 (17.1)	8 (66.7)	< 0.001
Pial invasion	0 (0)	1 (8.3)	0.011
T2-FLAIR mismatch	31 (40.8)	2 (16.7)	0.109
Proportion of enhancing tumor > 33%	17 (22.4)	10 (83.3)	< 0.001
Marked/avid enhancement	20 (26.3)	9 (75.0)	0.001
Presence of cyst	18 (23.7)	2 (16.7)	0.590
Proportion of necrosis > 5%	10 (13.2)	6 (50.0)	0.002
Infiltrative pattern	5 (6.6)	5 (41.7)	< 0.001
Maximal diameter, cm	5.70 ± 2.05	8.12 ± 1.88	0.005
Volume, cm^3	56.58 ± 51.85	115.87 ± 67.50	0.001
Mean ADC, x 10^{-3} mm^2/s	1.29 ± 0.22	1.10 ± 0.14	0.416
ADC 5th percentile, x 10^{-3} mm^2/s	0.86 ± 0.14	0.84 ± 0.07	0.442
Mean nCBV	1.72 ± 0.70	2.16 ± 1.26	0.056
nCBV 95th percentile	5.51 ± 2.14	7.71 ± 4.94	0.007

Data are either mean ± standard deviation or number with percentage in parentheses. *Calculated from chi-square test or Fisher' test for categorical variables, and independent t test or Mann-Whitney U-test for continuous variables according to normality. ADC = apparent diffusion coefficient, CDKN = cyclin-dependent kinase inhibitor, FLAIR = fluid-attenuated inversion recovery, IDH = isocitrate dehydrogenase, nCBV = normalized cerebral blood volume

https://doi.org/10.3348/kjr.2022.0732

Table 2. Logistic Regression Analysis for Clinical and Imaging Predictors of CDKN2A/B Homozygous Deletion Status in IDH-Mutant Astrocytomas in the Entire Patients

	Univariable		Multivariable	
	OR (95% CI)	*P*	OR (95% CI)	*P*
Age*	1.00 (0.95–1.06)	0.930		
Sex (female vs. male)†	0.84 (0.24–2.87)	0.777		
MRI features				
Frontal location (present vs. absent)†	1.62 (0.45–5.84)	0.462		
Cortical involvement (present vs. absent)†	0.61 (0.06–5.98)	0.672		
Corpus callosum involvement (present vs. absent)†	9.86 (2.50–38.91)	0.001	-	-
Ependymal extension (present vs. absent)†	9.69 (2.54–37.04)	0.001	-	-
Pial invasion (present vs. absent)†	-	NA		
T2-FLAIR mismatch (present vs. absent)†	0.29 (0.06–1.42)	0.126		
Proportion of enhancing tumor > 33% (present vs. absent)†	17.35 (3.46–86.92)	0.001	-	-
Marked/avid enhancement (present vs. absent)†	8.40 (2.07–34.16)	0.003	-	-
Presence of cyst (present vs. absent)†	0.64 (0.13–3.22)	0.592		
Proportion of necrosis > 5% (present vs. absent)†	6.60 (1.78–24.52)	0.005	-	-
Infiltrative pattern (present vs. absent)†	10.14 (2.35–43.79)	0.002	4.25 (1.47–37.85)	0.034
Maximal diameter (cm)*	1.06 (1.10–1.11)	0.004	1.07 (1.02–1.14)	0.013
Volume (cm^3)*	1.02 (1.00–1.05)	0.003	-	-
Mean ADC (x 10^{-3} mm^2/s)*	1.00 (1.00–1.00)	0.726		
ADC 5th percentile (x 10^{-3} mm^2/s)*	1.00 (1.00–1.01)	0.739		
Mean nCBV*	1.96 (0.89–4.29)	0.095		
nCBV 95th percentile*	1.27 (1.02–1.59)	0.012	1.34 (1.00–1.79)	0.049

*For continuous variables, an increase by 1 considered when calculating ORs and 95% CIs, †For categorical variables with categories in parentheses, the former was compared with the latter (the reference) to calculate ORs and 95% CIs. ADC = apparent diffusion coefficient, CDKN = cyclin-dependent kinase inhibitor, CI = confidence interval, FLAIR = fluid-attenuated inversion recovery, IDH = isocitrate dehydrogenase, NA = not available (due to complete separation), nCBV = normalized cerebral blood volume, OR = odds ratio

diameter (8.12 cm vs. 6.13 cm, $p = 0.028$), and 95th percentile of nCBV (7.71 vs. 5.60, $p = 0.030$) than those of IDH-mutant astrocytomas without CDKN2A/B homozygous deletion. There were no significant differences in other clinical and imaging parameters (Supplementary Table 3).

Supplementary Table 4 shows the results of univariable and multivariable analyses. In univariable analysis, corpus callosum involvement (OR = 6.00, $p = 0.017$), ependymal extension (OR = 4.36, $p = 0.039$), the proportion of enhancing tumor > 33% (OR = 5.29, $p = 0.049$), infiltrative pattern (OR = 5.54, $p = 0.030$), maximal diameter (OR = 1.04, $p = 0.039$), and 95th percentile of nCBV (OR = 1.24, $p = 0.037$) were predictors of CDKN2A/B homozygous deletion. On multivariable analysis, the infiltrative pattern (OR = 10.39, $p = 0.012$) and 95th percentile of nCBV (OR = 1.24, $p = 0.047$) were independent predictors of CDKN2A/B homozygous deletion. The AUC, accuracy, sensitivity, and specificity of the multivariable model were 0.76 (95% CI 0.60–0.88), 87.8%, 80.0%, and 58.1%, respectively. The ROC curves of the multivariable model are shown in Figure 4B.

DISCUSSION

In our study, the presence of an infiltrative pattern, larger maximal diameter, and higher 95th percentile of nCBV independently predicted CDKN2A/B homozygous deletion status, with an AUC of 0.83. In the subgroup analysis of histological grades 3 and 4 IDH-mutant astrocytomas, a similar result was observed; the presence of an infiltrative pattern and higher 95th percentile of nCBV independently predicted CDKN2A/B homozygous deletion status, with an AUC of 0.74. It is crucial to understand the imaging characteristics of this newly included entity in the 2021 WHO classification, as the presence of CDKN2A/B homozygous deletion is associated with poor prognosis in IDH-mutant astrocytomas of all grades [4,8,29]. Moreover, the predictive effect of CDKN2A/B homozygous deletion on therapeutic outcomes will likely be explored in future studies. Therefore, preoperative information on CDKN2A/B homozygous deletion status may be useful for guiding treatment decisions and predicting prognosis.

https://doi.org/10.3348/kjr.2022.0732

Korean Journal of Radiology
KJR

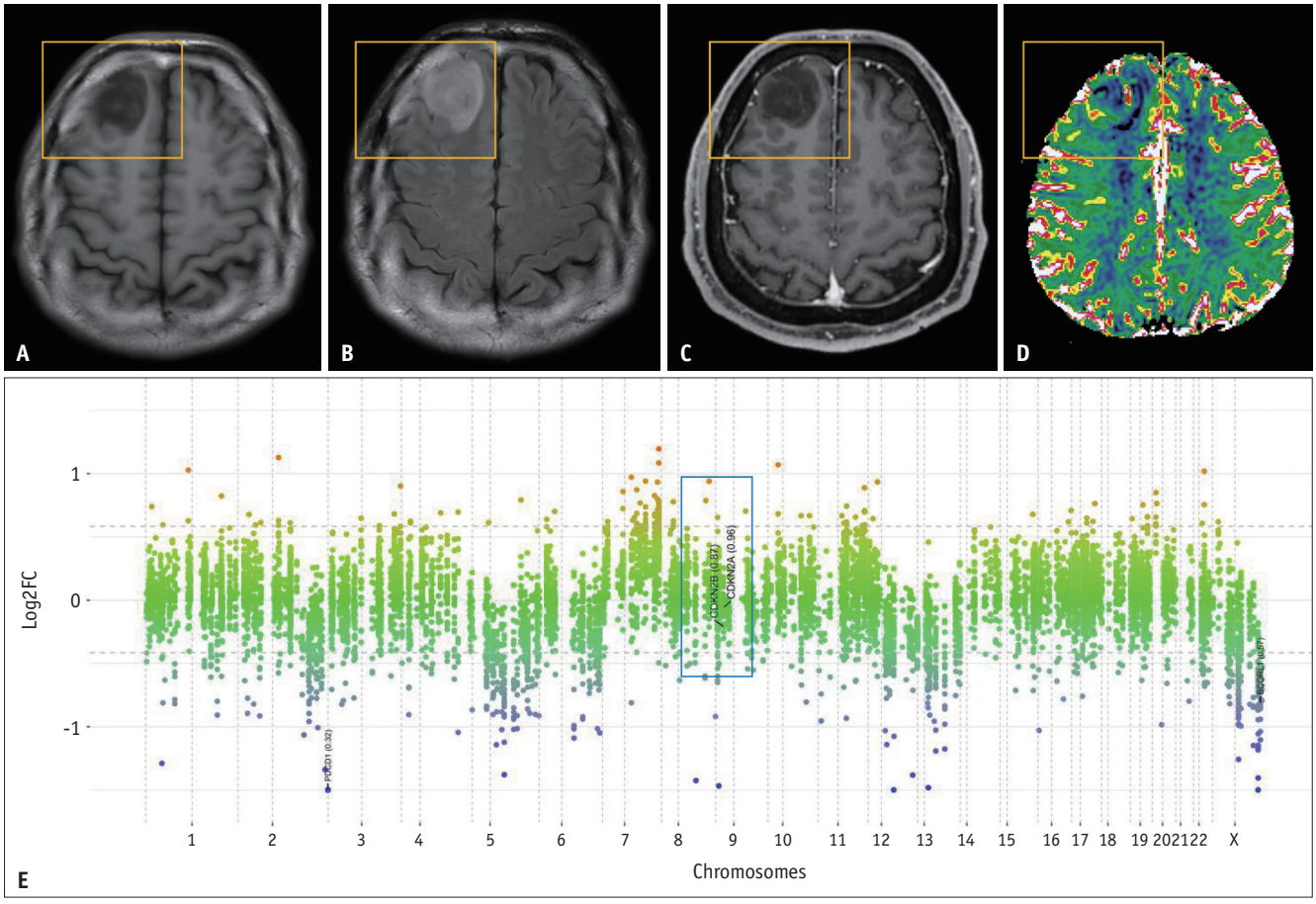

Fig. 2. Representative case of a 40-year-old male, histological grade 3 IDH-mutant astrocytoma without CDKN2A/B HD.
A-E. On **(A)** axial precontrast T1, **(B)** FLAIR, and **(C)** T1C images, a T2 hyperintense tumor of the right frontal lobe shows no evidence of corpus callosum involvement or ependymal extension. The proportion of enhancing tumors is less than 5% with minimal/mild enhancement. The tumor shows an expansive pattern (size of precontrast T1 abnormality approximates the size of FLAIR abnormality) with a maximal diameter of 2.40 cm. **(D)** The nCBV map shows the mean and 95th rCBV of 0.32 and 2.30, respectively. **(E)** The copy number variation profile shows an absence of CDKN2A/B HD. CDKN = cyclin-dependent kinase inhibitor, FLAIR = fluid-attenuated inversion recovery, HD = homozygous deletion, IDH = isocitrate dehydrogenase, nCBV = normalized cerebral blood volume, rCBV = relative cerebral blood volume, T1 = T1-weighted, T1C = postcontrast T1-weighted

Several earlier imaging studies, including both grade 4 IDH-mutant astrocytomas and IDH-wildtype glioblastomas (both classified as glioblastomas according to 2016 WHO classification), explored imaging findings associated with CDKN2A/B homozygous deletion [13,30,31], with conflicting results. One study showed that there was no difference in conventional imaging findings in grade 4 astrocytomas (including both IDH-mutant astrocytomas and IDH-wildtype glioblastomas) according to CDKN2A/B homozygous deletion status [13], whereas other studies have shown that aggressive conventional imaging features (such as necrosis or thickness of enhancing margin) were more frequent in the presence of CDKN2A/B homozygous deletions [30,31]. However, most tumors with CDKN2A/B homozygous deletion in previous studies were IDH-wildtype glioblastomas [31], and only a few conventional imaging parameters were evaluated in earlier studies. Currently, there are limited imaging reports reflecting the updated molecular markers in 2021 WHO classification; only a few recent studies have reported qualitative or quantitative imaging findings according to molecular markers in IDH-wild-type astrocytomas [14,32,33], whereas there is a lack of previous imaging studies based on molecular markers in IDH-mutant astrocytomas.

Although IDH-mutant astrocytomas are well known for their well-defined borders on MRI compared to those of IDH-wild-type astrocytomas [34], a substantial portion of IDH-mutant astrocytomas has also been reported to have an infiltrative pattern [22]. CDKN2A/B homozygous deletion alters inhibitory function in the cell cycle of

 https://doi.org/10.3348/kjr.2022.0732

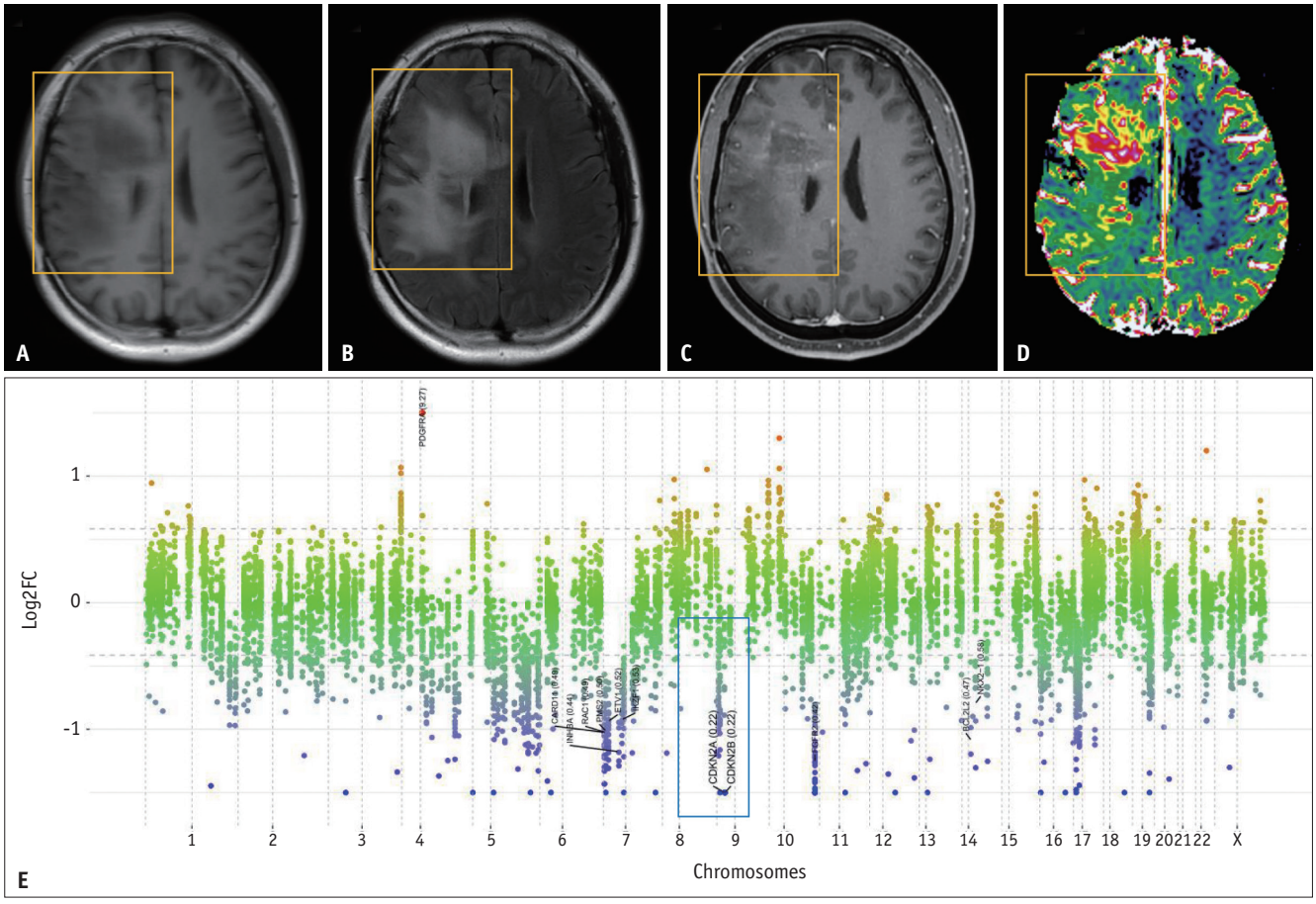

Fig. 3. Representative case of a 32-year-old male, histological grade 3 IDH-mutant astrocytoma with CDKN2A/B homozygous deletion.
A-E. On **(A)** axial precontrast T1, **(B)** FLAIR, and **(C)** T1C images, the right frontoparietal lobe T2 hyperintense tumor shows corpus callosum involvement and ependymal extension. The proportion of enhancing tumors is more than 5% with marked/avid enhancement. The tumor shows an infiltrative pattern (size of precontrast T1 abnormality much smaller than the size of FLAIR abnormality) with a maximal diameter of 8.70 cm. **(D)** The nCBV map shows the mean and 95th rCBV of 2.42 and 7.79, respectively. **(E)** The copy number variation profile shows the presence of CDKN2A/B homozygous deletion. FLAIR = fluid-attenuated inversion recovery, IDH = isocitrate dehydrogenase, nCBV = normalized cerebral blood volume, rCBV = relative cerebral blood volume, T1 = T1-weighted, T1C = postcontrast T1-weighted

tumor cells and contributes to uncontrolled tumor cell proliferation and increased tumorigenic burden [35]. This aggressive biological behavior may explain the infiltrative pattern of IDH-mutant astrocytomas with CDKN2A/B homozygous deletion in our study, which corresponds to previous pathology reports [36,37]. The infiltrative pattern on imaging has also been suggested to be correlated with more aggressive molecular phenotypes in either lower-grade gliomas or IDH-wild-type astrocytomas [22,33]. Earlier pathology studies in gliomas have shown that CDKN2A/B homozygous deletion is also associated with high proliferative indices [38,39], which may explain the larger maximal diameter in IDH-mutant astrocytomas with CDKN2A/B homozygous deletion. The higher 95th percentile of nCBV in IDH-mutant astrocytomas with CDKN2A/B may reflect increased angiogenesis due to CDKN2A/B homozygous deletion. The CDKN2A/B genetic locus encodes tumor suppressors that mediate anti-angiogenic effects in gliomas [40]. CDKN2A/B prevents tumor growth by limiting the supply of nutrients and oxygen to cancer cells and by inhibiting tumor-induced neovascularization [41]. CDKN2A/B homozygous deletion may lead to disinhibition of neovascularization. Conversely, ADC values did not reach statistical significance according to CDKN2A/B homozygous deletion status, although there was a trend of lower mean and 5th percentile of ADC values in IDH-mutant astrocytomas with CDKN2A/B, which warrants validation with a larger dataset.

In our study, subgroup analysis of histological grades 3 and 4 IDH-mutant astrocytomas was performed because of

https://doi.org/10.3348/kjr.2022.0732

Korean Journal of Radiology
KJR

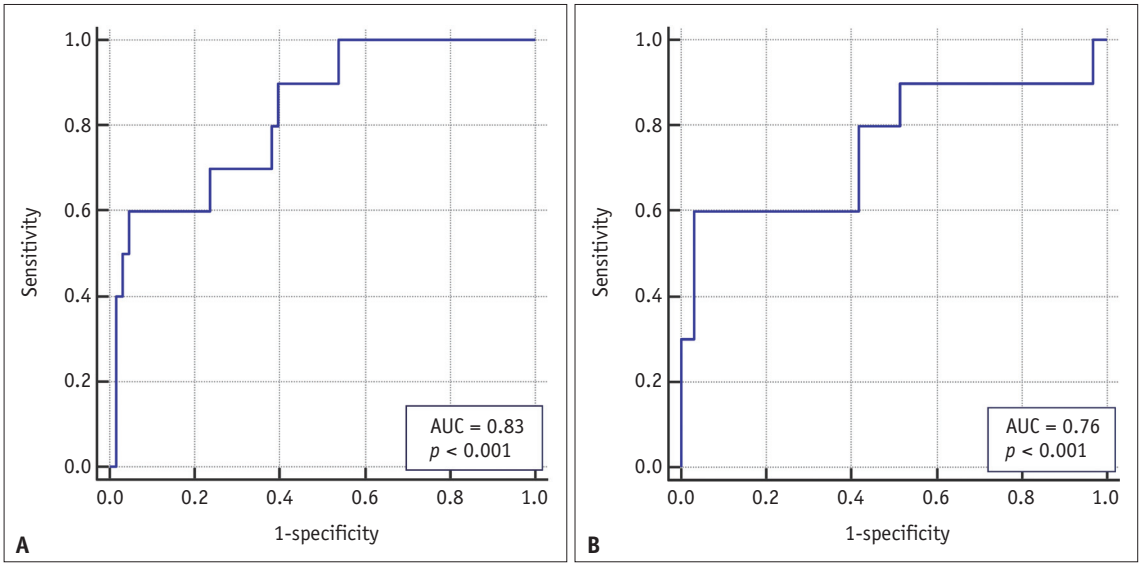

Fig. 4. Receiver operating characteristic curves of the multivariable models to predict the CDKN2A/B homozygous deletion status in (A) the entire patients and (B) a subgroup of patients with histological grades 3 and 4 IDH-mutant astrocytoma. AUC = area under the curve, CDKN = cyclin-dependent kinase inhibitor, IDH = isocitrate dehydrogenase

the lack of patients with CDKN2A/B homozygous deletions in histological grade 2 IDH-mutant astrocytomas. The data imbalance of CDKN2A/B is inevitable among histological grades in IDH-mutant astrocytomas; the reported frequencies of CDKN2A/B homozygous deletions range from 0%–12% in histological grade 2, 6%–20% in histological grade 3, and 16%–34% in histological grade 4 [4,8,29], which shows a similar distribution to our dataset. A similar result was observed in subgroup analyses, suggesting that the presence of CDKN2A/B homozygous deletion shows an aggressive pathological phenotype, even in higher histological grades. To exclude the possibility that the imaging features were affected by the histological grade, we performed a multicenter study to include as many patients as possible. Nonetheless, future studies with larger datasets are required.

Although the 2021 WHO classification of gliomas does not include neuroimaging features, previous research has suggested that neuroimaging may have a complementary role in identifying the molecular status of adult-type diffuse gliomas. In a previous study, the 1p/19q co-deletion status in IDH-mutant gliomas determined by chromosomal microarray analysis disagreed with the initial fluorescence in situ hybridization result and agreed with the consensus neuroradiologist prediction [42], which shows the additional role of MRI. Although the gold standard for copy number variant detection in CDKN2A/B is multiplex ligation-dependent probe amplification and array comparative genomic hybridization [43,44], these methods are time-consuming and costly, and NGS is more commonly used for diagnosis. As there is a small but significant rate of discordance in the methods for CDKN2A/B homozygous deletion testing [43], neuroimaging findings may assist in the diagnosis of discordant cases.

Our study had several limitations. First, it was retrospective and had a relatively small dataset. However, to the best of our knowledge, this is the largest multicenter dataset that includes both diffusion and perfusion parameters in IDH-mutant astrocytomas with a known CDKN2A/B homozygous deletion status. Second, prognostic markers were not analyzed because patients with IDH-mutant astrocytomas have relatively longer survival and require a longer follow-up period [45].

In conclusion, the presence of an infiltrative pattern, larger maximal diameter, and higher 95th percentile of the nCBV may be useful MRI biomarkers for CDKN2A/B homozygous deletion in IDH-mutant astrocytomas.

Supplement

The Supplement is available with this article at https://doi.org/10.3348/kjr.2022.0732.

Availability of Data and Material

The datasets generated or analyzed during the study are not publicly available due to institutional regulations but are available from the corresponding author on reasonable

request.

Conflicts of Interest

Ji Eun Park and Ho Sung Kim who is on the editorial board of the *Korean Journal of Radiology* was not involved in the editorial evaluation or decision to publish this article. All remaining authors have declared no conflicts of interest.

Author Contributions

Conceptualization: Yae Won Park, Se Hoon Kim. Data curation: Ki Sung Park, Ji Eun Park, Ho Sung Kim, Jong Hee Chang. Formal analysis: Yae Won Park. Funding acquisition: Yae Won Park. Investigation: Yae Won Park. Methodology: Yae Won Park. Project administration: Ki Sung Park. Resources: Ji Eun Park, Ho Sung Kim, Jong Hee Chang. Software: Ki Sung Park. Supervision: Seung-Koo Lee. Validation: Yae Won Park. Visualization: Yae Won Park, Se Hoon Kim. Writing—original draft: Yae Won Park, Se Hoon Kim. Writing—review & editing: Yae Won Park, Se Hoon Kim.

ORCID iDs

Yae Won Park
https://orcid.org/0000-0001-8907-5401
Ki Sung Park
https://orcid.org/0000-0002-7447-4247
Ji Eun Park
https://orcid.org/0000-0002-4419-4682
Sung Soo Ahn
https://orcid.org/0000-0002-0503-5558
Inho Park
https://orcid.org/0000-0003-2250-6507
Ho Sung Kim
https://orcid.org/0000-0002-9477-7421
Jong Hee Chang
https://orcid.org/0000-0003-1509-9800
Seung-Koo Lee
https://orcid.org/0000-0001-5646-4072
Se Hoon Kim
https://orcid.org/0000-0001-7516-7372

Funding Statement

This research was supported by Basic Science Research Program through the National Research Foundation of Korea (NRF) funded by the Ministry of Education (2020R1I1A1A01071648). This research was also supported by the "Team Science Award" of Yonsei University College of Medicine (6-2021-0009).

REFERENCES

1. Louis DN, Perry A, Wesseling P, Brat DJ, Cree IA, Figarella-Branger D, et al. The 2021 WHO classification of tumors of the central nervous system: a summary. *Neuro Oncol* 2021;23:1231-1251
2. Louis DN, Wesseling P, Aldape K, Brat DJ, Capper D, Cree IA, et al. cIMPACT-NOW update 6: new entity and diagnostic principle recommendations of the cIMPACT-Utrecht meeting on future CNS tumor classification and grading. *Brain Pathol* 2020;30:844-856
3. Cimino PJ, Holland EC. Targeted copy number analysis outperforms histologic grading in predicting patient survival for WHO grades II/III IDH-mutant astrocytomas. *Neuro Oncol* 2019;21:819-821
4. Aoki K, Nakamura H, Suzuki H, Matsuo K, Kataoka K, Shimamura T, et al. Prognostic relevance of genetic alterations in diffuse lower-grade gliomas. *Neuro Oncol* 2018;20:66-77
5. Olar A, Wani KM, Alfaro-Munoz KD, Heathcock LE, van Thuijl HF, Gilbert MR, et al. IDH mutation status and role of WHO grade and mitotic index in overall survival in grade II-III diffuse gliomas. *Acta Neuropathol* 2015;129:585-596
6. Reuss DE, Mamatjan Y, Schrimpf D, Capper D, Hovestadt V, Kratz A, et al. IDH mutant diffuse and anaplastic astrocytomas have similar age at presentation and little difference in survival: a grading problem for WHO. *Acta Neuropathol* 2015;129:867-873
7. Reis GF, Pekmezci M, Hansen HM, Rice T, Marshall RE, Molinaro AM, et al. CDKN2A loss is associated with shortened overall survival in lower-grade (World Health Organization grades II-III) astrocytomas. *J Neuropathol Exp Neurol* 2015;74:442-452
8. Shirahata M, Ono T, Stichel D, Schrimpf D, Reuss DE, Sahm F, et al. Novel, improved grading system(s) for IDH-mutant astrocytic gliomas. *Acta Neuropathol* 2018;136:153-166
9. Foulkes WD, Flanders TY, Pollock PM, Hayward NK. The CDKN2A (p16) gene and human cancer. *Mol Med* 1997;3:5-20
10. Sherr CJ. Cancer cell cycles. *Science* 1996;274:1672-1677
11. Alhejaily A, Day AG, Feilotter HE, Baetz T, Lebrun DP. Inactivation of the CDKN2A tumor-suppressor gene by deletion or methylation is common at diagnosis in follicular lymphoma and associated with poor clinical outcome. *Clin Cancer Res* 2014;20:1676-1686
12. van den Bent MJ, Afra D, de Witte O, Ben Hassel M, Schraub S, Hoang-Xuan K, et al. Long-term efficacy of early versus delayed radiotherapy for low-grade astrocytoma and oligodendroglioma in adults: the EORTC 22845 randomised trial. *Lancet* 2005;366:985-990
13. Gutman DA, Cooper LA, Hwang SN, Holder CA, Gao J, Aurora TD, et al. MR imaging predictors of molecular profile and survival: multi-institutional study of the TCGA glioblastoma data set. *Radiology* 2013;267:560-569
14. Park YW, Ahn SS, Park CJ, Han K, Kim EH, Kang SG, et al. Diffusion and perfusion MRI may predict EGFR amplification and the TERT promoter mutation status of IDH-wildtype

lower-grade gliomas. *Eur Radiol* 2020;30:6475-6484
15. Choi KS. Deep learning applications in perfusion MRI: recent advances and current challenges. *Investig Magn Reson Imaging* 2022;26:246-255
16. Pak E, Choi SH, Park CK, Kim TM, Park SH, Won JK, et al. Added value of contrast leakage information over the CBV value of DSC perfusion MRI to differentiate between pseudoprogression and true progression after concurrent chemoradiotherapy in glioblastoma patients. *Investig Magn Reson Imaging* 2022;26:10-19
17. Yan H, Parsons DW, Jin G, McLendon R, Rasheed BA, Yuan W, et al. IDH1 and IDH2 mutations in gliomas. *N Engl J Med* 2009;360:765-773
18. Riemenschneider MJ, Jeuken JW, Wesseling P, Reifenberger G. Molecular diagnostics of gliomas: state of the art. *Acta Neuropathol* 2010;120:567-584
19. Boxerman JL, Schmainda KM, Weisskoff RM. Relative cerebral blood volume maps corrected for contrast agent extravasation significantly correlate with glioma tumor grade, whereas uncorrected maps do not. *AJNR Am J Neuroradiol* 2006;27:859-867
20. Cha J, Kim ST, Kim HJ, Kim BJ, Kim YK, Lee JY, et al. Differentiation of tumor progression from pseudoprogression in patients with posttreatment glioblastoma using multiparametric histogram analysis. *AJNR Am J Neuroradiol* 2014;35:1309-1317
21. Maes F, Collignon A, Vandermeulen D, Marchal G, Suetens P. Multimodality image registration by maximization of mutual information. *IEEE Trans Med Imaging* 1997;16:187-198
22. Park YW, Han K, Ahn SS, Bae S, Choi YS, Chang JH, et al. Prediction of IDH1-mutation and 1p/19q-codeletion status using preoperative MR imaging phenotypes in lower grade gliomas. *AJNR Am J Neuroradiol* 2018;39:37-42
23. Patel SH, Poisson LM, Brat DJ, Zhou Y, Cooper L, Snuderl M, et al. T2-FLAIR mismatch, an imaging biomarker for IDH and 1p/19q status in lower-grade gliomas: a TCGA/TCIA project. *Clin Cancer Res* 2017;23:6078-6085
24. Kickingereder P, Isensee F, Tursunova I, Petersen J, Neuberger U, Bonekamp D, et al. Automated quantitative tumour response assessment of MRI in neuro-oncology with artificial neural networks: a multicentre, retrospective study. *Lancet Oncol* 2019;20:728-740
25. Isensee F, Jäger PF, Kohl SA, Petersen J, Maier-Hein KH. Automated design of deep learning methods for biomedical image segmentation. arXiv [Preprint]. 2019 [cited 2022 November 11]. Available at: https://doi.org/10.48550/arXiv.1904.08128
26. Park YW, Eom J, Kim D, Ahn SS, Kim EH, Kang SG, et al. A fully automatic multiparametric radiomics model for differentiation of adult pilocytic astrocytomas from high-grade gliomas. *Eur Radiol* 2022;32:4500-4509
27. Choi HJ, Choi SH, You SH, Yoo RE, Kang KM, Yun TJ, et al. MGMT promoter methylation status in initial and recurrent glioblastoma: correlation study with DWI and DSC PWI features. *AJNR Am J Neuroradiol* 2021;42:853-860
28. Chu HH, Choi SH, Ryoo I, Kim SC, Yeom JA, Shin H, et al. Differentiation of true progression from pseudoprogression in glioblastoma treated with radiation therapy and concomitant temozolomide: comparison study of standard and high-b-value diffusion-weighted imaging. *Radiology* 2013;269:831-840
29. Yang RR, Shi ZF, Zhang ZY, Chan AK, Aibaidula A, Wang WW, et al. IDH mutant lower grade (WHO grades II/III) astrocytomas can be stratified for risk by CDKN2A, CDK4 and PDGFRA copy number alterations. *Brain Pathol* 2020;30:541-553
30. Kickingereder P, Bonekamp D, Nowosielski M, Kratz A, Sill M, Burth S, et al. Radiogenomics of glioblastoma: machine learning–based classification of molecular characteristics by using multiparametric and multiregional MR imaging features. *Radiology* 2016;281:907-918
31. Ahn SS, An C, Park YW, Han K, Chang JH, Kim SH, et al. Identification of magnetic resonance imaging features for the prediction of molecular profiles of newly diagnosed glioblastoma. *J Neurooncol* 2021;154:83-92
32. Park CJ, Han K, Kim H, Ahn SS, Choi D, Park YW, et al. MRI features may predict molecular features of glioblastoma in isocitrate dehydrogenase wild-type lower-grade gliomas. *AJNR Am J Neuroradiol* 2021;42:448-456
33. Park YW, Park JE, Ahn SS, Kim EH, Kang SG, Chang JH, et al. Magnetic resonance imaging parameters for noninvasive prediction of epidermal growth factor receptor amplification in isocitrate dehydrogenase-wild-type lower-grade gliomas: a multicenter study. *Neurosurgery* 2021;89:257-265
34. Suh CH, Kim HS, Jung SC, Choi CG, Kim SJ. Imaging prediction of isocitrate dehydrogenase (IDH) mutation in patients with glioma: a systemic review and meta-analysis. *Eur Radiol* 2019;29:745-758
35. Lu VM, O'Connor KP, Shah AH, Eichberg DG, Luther EM, Komotar RJ, et al. The prognostic significance of CDKN2A homozygous deletion in IDH-mutant lower-grade glioma and glioblastoma: a systematic review of the contemporary literature. *J Neurooncol* 2020;148:221-229
36. Aibaidula A, Chan AK, Shi Z, Li Y, Zhang R, Yang R, et al. Adult IDH wild-type lower-grade gliomas should be further stratified. *Neuro Oncol* 2017;19:1327-1337
37. Brat DJ, Verhaak RG, Aldape KD, Yung WK, Salama SR, Cooper LA, et al. Comprehensive, integrative genomic analysis of diffuse lower-grade gliomas. *N Engl J Med* 2015;372:2481-2498
38. Ono Y, Tamiya T, Ichikawa T, Kunishio K, Matsumoto K, Furuta T, et al. Malignant astrocytomas with homozygous CDKN2/p16 gene deletions have higher Ki-67 proliferation indices. *J Neuropathol Exp Neurol* 1996;55:1026-1031
39. Labuhn M, Jones G, Speel EJ, Maier D, Zweifel C, Gratzl O, et al. Quantitative real-time PCR does not show selective targeting of p14(ARF) but concomitant inactivation of both p16(INK4A) and p14(ARF) in 105 human primary gliomas. *Oncogene* 2001;20:1103-1109

40. Zerrouqi A, Pyrzynska B, Febbraio M, Brat DJ, Van Meir EG. P14ARF inhibits human glioblastoma-induced angiogenesis by upregulating the expression of TIMP3. *J Clin Invest* 2012;122:1283-1295
41. Folkman J. Role of angiogenesis in tumor growth and metastasis. *Semin Oncol* 2002;29(6 Suppl 16):15-18
42. Patel SH, Batchala PP, Mrachek EKS, Lopes MS, Schiff D, Fadul CE, et al. MRI and CT identify isocitrate dehydrogenase (IDH)-mutant lower-grade gliomas misclassified to 1p/19q codeletion status with fluorescence in situ hybridization. *Radiology* 2020;294:160-167
43. Kerkhof J, Schenkel LC, Reilly J, McRobbie S, Aref-Eshghi E, Stuart A, et al. Clinical validation of copy number variant detection from targeted next-generation sequencing panels. *J Mol Diagn* 2017;19:905-920
44. Talevich E, Shain AH, Botton T, Bastian BC. CNVkit: genome-wide copy number detection and visualization from targeted DNA sequencing. *PLoS Comput Biol* 2016;12:e1004873
45. Kim M, Kim S, Park YW, Han K, Ahn SS, Moon JH, et al. Sex as a prognostic factor in adult-type diffuse gliomas: an integrated clinical and molecular analysis according to the 2021 WHO classification. *J Neurooncol* 2022;159:695-703

https://doi.org/10.3348/kjr.2022.0732